Signal Amplification and Near-Infrared Translation of Enzymatic Reactions by Nanosensors

Justus T. Metternich[a,b], Björn Hill[a], Janus A.C. Wartmann[a], Chen Ma[a], Rebecca M. Kruskop[b], Krisztian Neutsch[a], Svenja Herbertz[b], Sebastian Kruss[a,b,c]

[a] Department of Chemistry, Ruhr-University Bochum, Universitätsstrasse 150, 44801 Bochum, Germany

[b] Biomedical Nanosensors, Fraunhofer Institute for Microelectronic Circuits and Systems, Finkenstrasse 61, 47057 Duisburg, Germany

[c] Center for Nanointegration Duisburg-Essen (CENIDE), Carl-Benz-Strasse 199, 47057 Duisburg, Germany

[*] Email: sebastian.kruss@rub.de.

Abstract

Enzymatic reactions are used to detect analytes in a range of biochemical methods such as enzyme-linked immunosorbent assays (ELISAs). To measure the presence of an analyte, they are conjugated to a recognition unit and convert a substrate into a (colored) product that is detectable by visible (VIS) light. Thus, the lowest enzymatic turnover that can be detected sets a limit on sensitivity. Here, we report that substrates and products of horseradish peroxidase (HRP) and β-galactosidase change the near-infrared (NIR, 800-2400 nm) fluorescence of (bio)polymer modified single-walled carbon nanotubes (SWCNTs). Therefore, SWCNTs translate a VIS signal into a beneficial NIR signal. Moreover, the affinity of the nanosensors cause a higher effective local concentration of the reactants for the optical measurement. This leads to a non-linear sensor-based signal amplification and translation (SENSAT). We find signal enhancement up to ≈ 120x for the HRP substrate *p*-phenylenediamine (PPD), which means that reactions below the limit of detection in the VIS can be followed in the NIR (≈ 1000 nm). The approach is also applicable to other substrates such as *3,3'-5,5'*-tetramethylbenzidine (TMB) and direct observation of the HRP reaction. An adsorption-based theoretical model fits the observed signals and corroborates the sensor-based enhancement mechanism. This approach can be used to amplify signals, translate them into the NIR and increase sensitivity of biochemical assays.

Keywords

Biosensors, Carbon nanotubes, Enzymes, Fluorescence, Near-Infrared

Introduction

Proteins are central building blocks in living organisms. In diseases, they are frequently mutated, misfolded, truncated or their concentration is different.[1] Accordingly, they present an important biomarker for diagnostic applications and basic research.[1] Standard techniques for the detection of proteins use enzymatic reactions. Prominent examples are enzyme-linked immunosorbent assays (ELISA)[2,3] or western blots[4–7]. In both techniques, the protein analyte is bound on a surface by a capture antibody and subsequently visualized with a second antibody conjugated to an enzyme.[1,8,9] The most common enzymes used in these reactions are horseradish peroxidase (HRP), alkaline phosphatase and β-galactosidase.[1] They catalyze the reaction of a colorless substrate into a colored product with known absorption in the visible range of the spectrum.

In order to increase the sensitivity of these assays, a number of alternative signal transduction mechanisms have been demonstrated. Examples include the use of femotliter (fL) detection volumes[10–12], or signal conversion with nanomaterials[13–18]. Nevertheless, the traditionally used absorption-based detection methods still represent the gold standard[19], especially in low budget settings. As such, ELISAs are often restricted by their sensitivity as well as their dynamic range and a method to extend the dynamic range of this assay system would be highly beneficial.

One option could be the addition of an additional molecule or particle that is highly sensitive to its chemical environment and amplifies the response generated during the enzymatic reaction. Such a method would require minimal adaption of assays as the signal amplifier could be added during the read-out step. Carbon nanotubes are cylindrical 1D materials with exceptional optoelectronic properties. Semiconducting single-walled carbon nanotubes (SWCNTs) do not photo-bleach and fluoresce in the near-infrared region (NIR, 870-2400 nm).[20] In this spectral window, the absorption, scattering and autofluorescence of biological samples is reduced.[21,22] Depending on the application, different spectral ranges are advantageous.[23] Moreover, the fluorescence of SWCNTs is sensitive to the chemical environment.[24] As such, they present an interesting building block for fundamental studies[25–27] and have been used in a variety of optical[24,28–30] and electrochemical[18,31] biosensing formats.

To render them capable for the detection of analytes, SWCNTs are functionalized with (bio)polymers.[32–35] When confined to the surface, the polymer forms pockets that selectively interact with analytes.[36–38] This concept has been called corona phase molecular recognition (CoPhMoRe).[36] Functionalization of SWCNTs has led to a number of powerful sensors for proteins and peptides,[39–48] nucleic acids[49–55], different neurotransmitters[23,56–59], radical species[60–65] and other small molecules[66–71] that possess sensing capabilities down to the single-molecule level[72–75].

Here, we show that fluorescent nanosensors amplify the signal of enzymatic reactions typically used in ELISAs. To this end, we identify SWCNT surface modifications that are sensitive to substrates or products of important enzymes (β-galactosidase and horseradish peroxidase). We investigate how the signal scales with analyte concentration and develop a theoretical model for signal enhancement. This approach presents a generic concept to increase chemical signals and translate it into a beneficial spectral window.

Results

We hypothesized that the aromatic structure of many colored enzymatic substrates and products of ELISAs/western blots could interact with the hydrophobic surface of SWCNTs. As the fluorescence of SWCNTs is highly sensitive to the chemical environment this would translate into fluorescent changes in the beneficial NIR spectral window (Figure 1). Furthermore, if the modified SWCNT surface has a certain affinity for the analyte, the local 'effective' concentration of the analyte should be higher (in terms of the optical measurement) than in bulk and therefore higher sensitivities are expected. Compared to other techniques requiring major adaptation of the assay, this system could be combined with advanced coating[59] and read-out[23] techniques and amplify signals of reactions used for *in vitro* diagnostics.

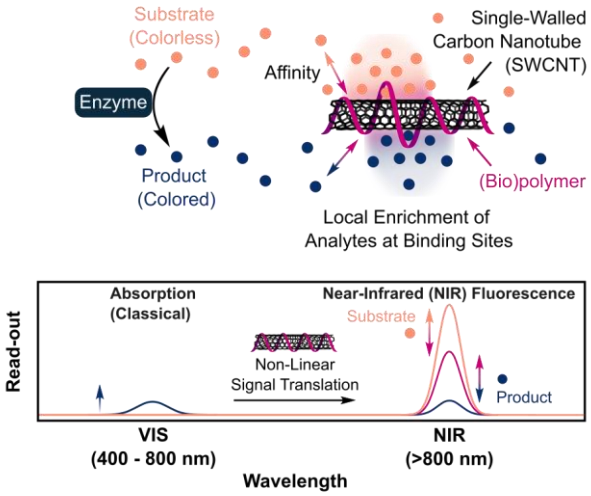

Figure 1: Sensor-based signal amplification and translation (SENSAT) of enzymatic reactions by nanosensors. In diagnostic assays, enzymatic reactions are commonly used to quantify the concentration of an analyte. To this end, they are attached to antibodies that bind to the target molecule and convert a (colorless) substrate into a colored product. The NIR-fluorescence of single-walled carbon nanotubes (SWCNTs) can be tailored to be sensitive to certain small molecules. Such a SWCNT-biopolymer hybrid with affinity for specific analytes could translate the signal into the NIR and amplify it by local analyte enrichment.

To test this hypothesis, SWCNTs were suspended with phospholipid-polyethylene glycol (PEG-PL) and different nucleic acids (Figure 1, Table S1). Subsequently, we tested whether the fluorescence changes of these hybrid nanomaterials would be selective for molecules of interest. For the enzyme HRP, we selected *o*- and *p*-phenylenediamine (OPD and PPD), as well as their respective reaction products 2,3-diaminophenanzine and Bandrowski's base (BB). The selection of these substrate/product pairs was based on the premise that the substrate and the product differ significantly in their size and molecular structure which could lead to different affinities for the SWCNT surface. We expected that these molecules change the DNA conformation, which would cause a change in fluorescence. Additionally, we tested the response of three different benzidine derivatives, which form colored radicals when oxidized by HRP and H_2O_2. Among them, we included *3,3'-5,5'*-tetramethylbenzidine (TMB), the most commonly used HRP substrate.[19] Apart from the popularity of these substrates, it is well established that these molecules are oxidized over different radical species while the product is typically a charged complex with increased rigidity. For SWCNTs, it is well known that radical species modulate the SWCNT response.[60,61,63,64,76] Furthermore, we expect that the enzymatic product affects the SWCNT conformation thereby leading to a fluorescent response. For the enzyme β-galactosidase, we tested the response to ortho-nitrophenyl-β-galactoside (OPNG)

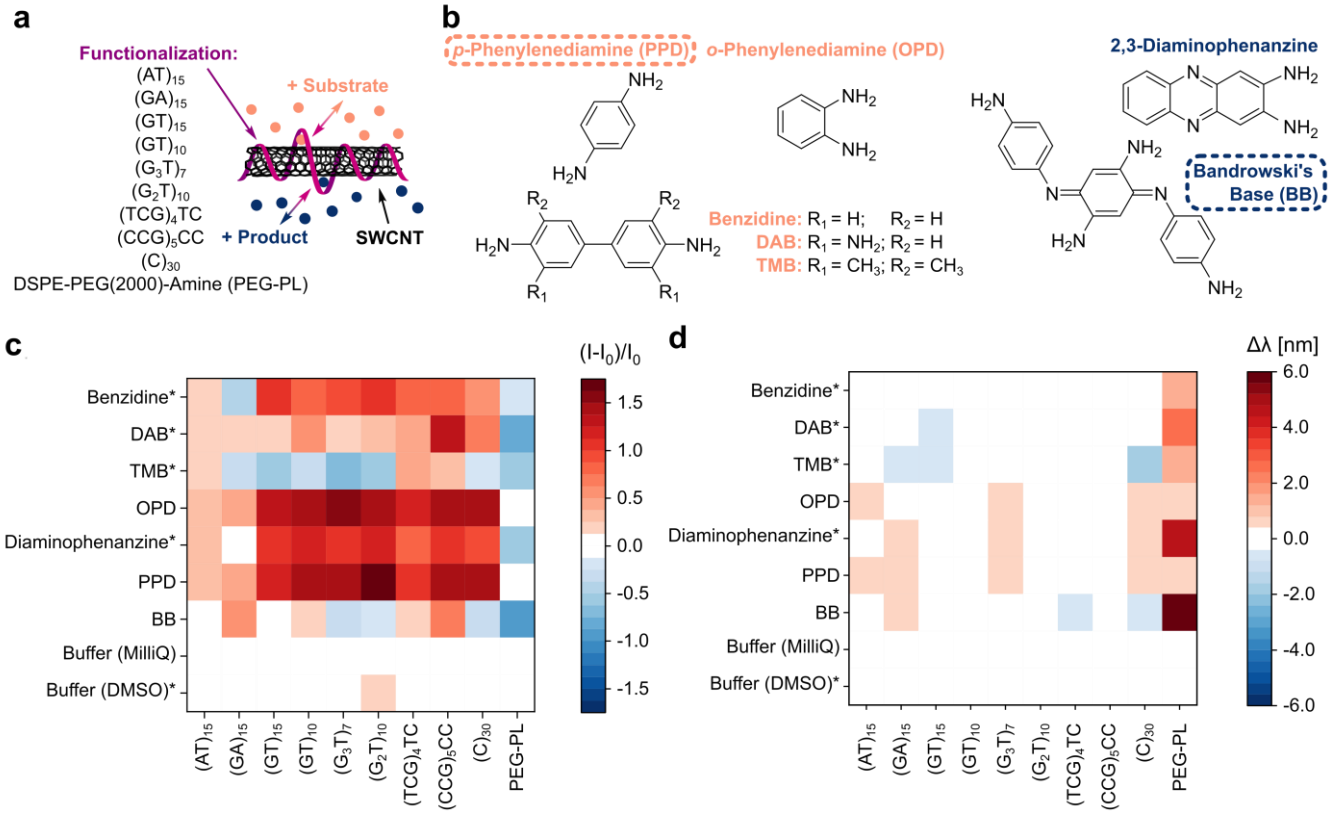

Figure 2: Horseradish peroxidase (HRP) substrates and products change NIR fluorescence of SWCNTs. (a) Overview of tested SWCNT surface modifications. (b) Selected structures of used HRP substrates (orange) and oxidation products (blue). (c) Intensity modulation ($[I-I_0]/I_0$) of NIR-fluorescent SWCNT sensors in response to HRP substrate and products (10 µM; mean, n=3; SD shown in Figure S2). Red shades indicate a fluorescence increase, blue shades indicate a fluorescence decrease. (d) Wavelength shifts (Δλ) of SWCNT sensors in response to HRP substrate and products (10 µM; mean, n=3, SD shown in Figure S2). Red shades indicate red shift of the fluorescence, blue shades indicate a blue shift. Based on the fluorescence modulation and the final chemical structure of the final product, we selected PPD/BB for future experiments (see molecules in (b) with dotted frame).

and chlorophenol red-β-D-galactopyranoside (CPRG), as well as their respective reaction products.

The addition of 10 µM substrate/product modified the fluorescence of the modified SWCNTs by up to + 164 % in the case of PPD (substrate) and - 87 % for BB (respective product). Furthermore, the emission maxima shifted up to 5.8 nm towards higher and 1.7 nm towards lower wavelengths. Generally, the addition of HRP substrates/products (Figure 2, Figure S1) affected the fluorescence to a higher degree than the addition of β-galactosidase substrates (Figure S2 and S3). The most sensitive pair was PPD and BB. Contrary to benzidine substrates, which form radical products when converted with HRP, this system allowed us to characterize the fluorescence modulation of SWCNTs via a substrate/product system in an enzymatically independent way before moving to an enzymatic reaction. Therefore, some of the modified SWCNTs can serve as nanosensors to monitor enzymatic reactions.

To test whether the response would be concentration dependent, we spiked two SWCNT suspensions with different concentrations of this analyte pair. For PEG-PL-SWCNTs, solely the enzymatic product (BB) lead to a fluorescent change (Figure 3a). Additionally, we observed no absorption of the corresponding substrate (PPD) in the visible spectrum (Figure 3b and S4). This allowed us to estimate the response during the enzymatic reaction based on the BB concentration. Compared to the traditional read-out format, the PEG-PL SWCNTs responded to 5 - 10x lower BB concentrations (Figure 3c).

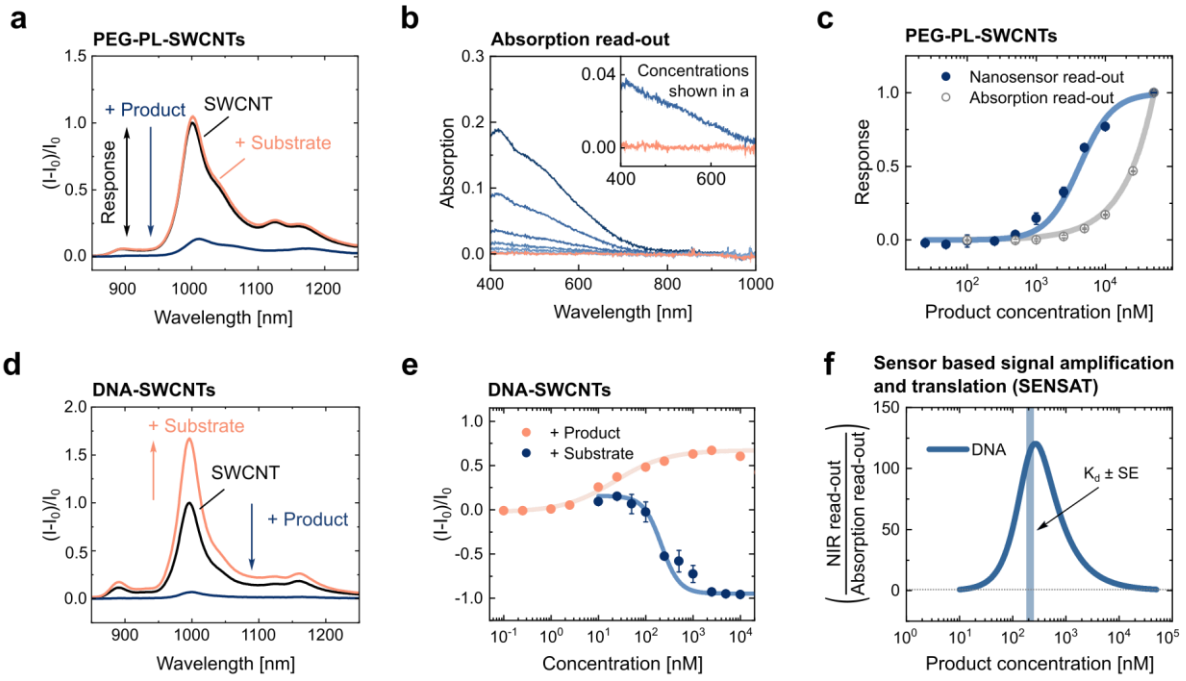

Figure 3: Range extension of detection by SWCNT-based nanosensors. (a) Fluorescence modulation of PEG-PL coated SWCNTs by PPD (10 µM, HRP substrate) and the respective reaction product (BB, 10 µM). (b) Absorption of PPD (pink, 10 µM) and BB (blue, from dark blue to light blue 50, 25, 10, 5, 2.5, 1 µM; n=3, mean ± SD). (c) Concentration dependent comparison of traditional read-out of BB (absorption changes at 500 nm, normalized to value at 50 µM) and respective fluorescence modulation of PEG-PL-SWCNTs (1 nM, $((I-I_0)/I_0$ normalized to value at 50 µM)). Note that PPD was not detectable in the VIS and only marginally modified the fluorescence. Thus, only the read-outs of BB are shown for simplicity (n=3, mean ± SD, raw data in Figure S6). (d) $(G_2T)_{10}$-modified SWCNT (0.1 nM) respond to the substrate and the product (both 10 µM, n=3, mean ± SD). (e) Concentration-dependent fluorescence changes of $(G_2T)_{10}$-modified SWCNTs (n=3, mean ± SD, normalized data in Figure S7). (f) The relative read-outs define the window for the sensor-based signal amplification (SENSAT) for $(G_2T)_{10}$-modified SWCNTs (≈ 120x). Note that the calculated signal amplification is only based on the product (substrate is not detectable in an absorption read-out). We expect that the nanosensor sensitivity for the substrate further enhances the observed signal amplification. Fits are linear for absorption data and modified Langmuir adsorption model (see text) with an offset for nanosensor responses (Fit parameters: Table S2-S3, SENSAT for PEG-PL in Figure S6c).

Interestingly, ssDNA-SWCNT hybrid sensors responded to both, the substrate (PPD) and the reaction product (BB) (Figure 3d-e). Furthermore, they were more sensitive than SWCNTs modified with PEG-PL. For PPD, first effects were seen at concentrations > 2.5 nM and the response saturated at concentrations of 2.5 µM, thereby spanning approximately three orders of magnitude. For BB, dose-dependent effects were observed > 50 nM while 5 µM quenched the fluorescence almost completely. Compared to the read-out in the visible (only BB detectable) this shift the detection limit to approximately 50x lower concentrations.

Interestingly, we observed a non-linear dependency between the responses generated with the classical and the NIR translated read-out. Due to the different magnitudes for PEG-PL- and DNA-modified sensors, we hypothesized that this dependency is based on the affinity of the substrate/product for the nanosensor. We call this mechanism sensor-based signal amplification and translation (SENSAT). It should be generic for any fluorescent material or molecule with a certain affinity for the analyte. Hence, we were interested to better understand the magnitude of amplification. To this end, we normalized the response generated by the nanosensor and the absorption read-out (Figure 3c, Figure S6). To be able to compare the different signals, both data sets were normalized (see SI for details). As expected from Lambert-Beer's law, the absorption data can be accurately described with a linear equation (Table S3).

In contrast, fluorescence modulation of SWCNTs should be proportional to surface coverage (θ).[56] We assumed a reversible binding between analyte (A) and recognition sites (R) on the nanosensor:

$$\mathrm{A} + \mathrm{R} \rightleftarrows \mathrm{AR}.$$

Then, the (relative) surface coverage θ can be described with a Langmuir adsorption model:

$$\theta = \frac{[A]}{K_d + [A]}$$

where [A] is the analyte concentration and K_d is the dissociation constant. As the photophysical translation of a binding event depends on the exciton diffusion length, as well as the exciton size, we assumed a non-linear relationship (exponent n) between the observed fluorescence change ($[I-I_0]/I_0$) and the surface coverage. Incorporating a factor to account for the offset factor between the end (I_E) and the non-zero start response/signal (I_S) of the sensors we get:

$$\frac{(\mathrm{I}-\mathrm{I}_0)}{\mathrm{I}_0} = \mathrm{I}_\mathrm{S} + (\mathrm{I}_\mathrm{E} - \mathrm{I}_\mathrm{S})\theta^n \,.$$

This model described and fitted our data very-well (Figure 3, Table S2). The ratio between the fitted NIR signal and the fit of the normalized absorption yields the signal amplification (SA) (details in SI):

$$\mathrm{SA} = \frac{\text{NIR-signal}}{\text{Absorption}} = I_S + (I_E - I_S)\frac{\left(\frac{[A]}{K_d + [A]}\right)^{\mathrm{n}}}{a + b[A]} \,.$$

Plotting the respective functions yields an enhancement factor of ≈ 6x for PEG-PL SWCNTs (Figure S6c) and ≈ 120x for $(G_2T)_{10}$-modified SWCNTs (Figure 3f) for BB. As PPD does not absorb in the visible, we had no reference value to compare the observed fluorescence enhancement with a traditional read-out. However, we expect that the consummation of the PPD during the enzymatic reaction reverses this positive modulation thereby amplifying the negative signal generated from BB.

To explore the opportunities generated by the sensor-based signal enhancement during an enzymatic reaction, we next monitored the HRP-based oxidation of PPD to BB with different SWCNT surface modifications. As expected, the enzymatic turnover of the reaction led to a decrease of the fluorescence (Figure S8). Importantly, the fluorescence decreased only upon addition of all reaction components. At reaction times > 60 min, the effect of H_2O_2 was negligible suggesting that the observed response is caused by the formation of BB. Sensors which performed better in our initial screening (Figure 2, Figure S8) also allowed a more precise monitoring of the reaction. Furthermore, it was possible to follow the reaction when SWCNTs were immobilized (Figure S9). Combined with the 2D excitation-emission spectra (Figure S10), this suggests that the mechanism behind the fluorescence decrease is not aggregation based.

To avoid desorption effects during the next experiments, we turned our interest to solution-based experiments. In solution, we observed that low SWCNT concentrations lead to a higher signal change and that high PPD ratios lead to a decrease of the SWCNT response beyond the saturation of the sensor (Figure S11). To minimize this effect, we adjusted the concentration ratio accordingly.

To showcase the sensitivity of the nanosensors, we first ran the HRP-catalyzed oxidation reaction at PPD concentrations that were below the detection limit of a classical plate reader (Figure 4d - f, Figure S4). Along with the fluorescent decrease we observed a blue shift that

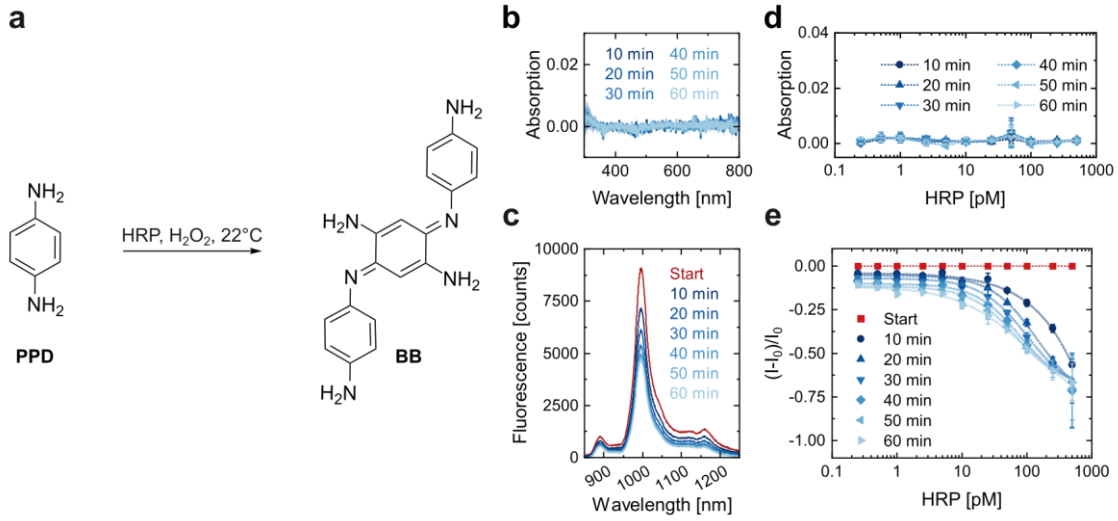

Figure 4: NIR monitoring of HRP reactions at concentrations below the detection limit of absorption measurements. (a) Reaction scheme of the PPD oxidation. (b) Conventional, absorption-based read-out below the absorption-based detection limit of the substrate/product. The reaction of PPD (1 µM), H_2O_2 (100 µM) and HRP (100 pM) was carried out without SWCNTs (n=3, mean ± SD). (c) Fluorescent changes of $(G_2T)_{10}$-SWCNTs (0.1 nM) during the same reaction with SWCNTs (n=3, mean ± SD). (d) Absorption changes during the reaction with varying HRP concentrations at 500 nm, the absorption maximum of Bandrowski's base (n=3, mean ± SD). (e) Fluorescence intensity changes of the reaction with varying HRP concentrations (n=3, mean ± SD). Fits are based on a modified Langmuir adsorption model (see text) with an offset. Wavelength shifts are shown in Figure S11.

correlated with the HRP concentration (Figure 4e and g, Figure S12). Interestingly, this peak shift seemed to be 5x to 10x times more sensitive than the intensity change. Together with the different equilibrium dynamics, this suggests a complex interplay between the different analytes and the binding sites on the SWCNT surface.

PPD and BB are classical ELISA reactants but in most current assays other molecules are used. Therefore, we tested next if it would be possible to use a substrate system with a broader use. Today, TMB is the most widely used substrate in ELISAs.[19] Its oxidation processes over a radical intermediate that can be followed at 370 nm/650 nm (TMB-I) and 450 nm (TMB-II) respectively (Figure 5a).[19,77,78]

To test how SWCNTs with different surface modifications would respond to the formation of oxidized TMB products, we incubated TMB for 30 min with HRP and H_2O_2, with H_2O_2, as well as without HRP and H_2O_2 and stopped the reaction with H_2SO_4 (50 µL, 1M). Addition of 2 µL of the reaction mixtures without HRP generally led to a fluorescence increase, while a fluorescent decrease was observed for reactions in which the enzyme was present (Figure 5b). Based on the fluorescent changes, we selected $(C)_{30}$-modified SWCNTs for our next experiments.

We observed a similar product conversion for mixtures that were illuminated with light matching the excitation of SWCNTs and those that were stored in the dark (Figure S13). This suggests that a potential oxidation of the TMB by an excited state of the SWCNT is not likely. Next, we repeated the reaction with different HRP concentrations (Figure 5c – d). As expected, we observed a concentration dependent decrease of the fluorescence.

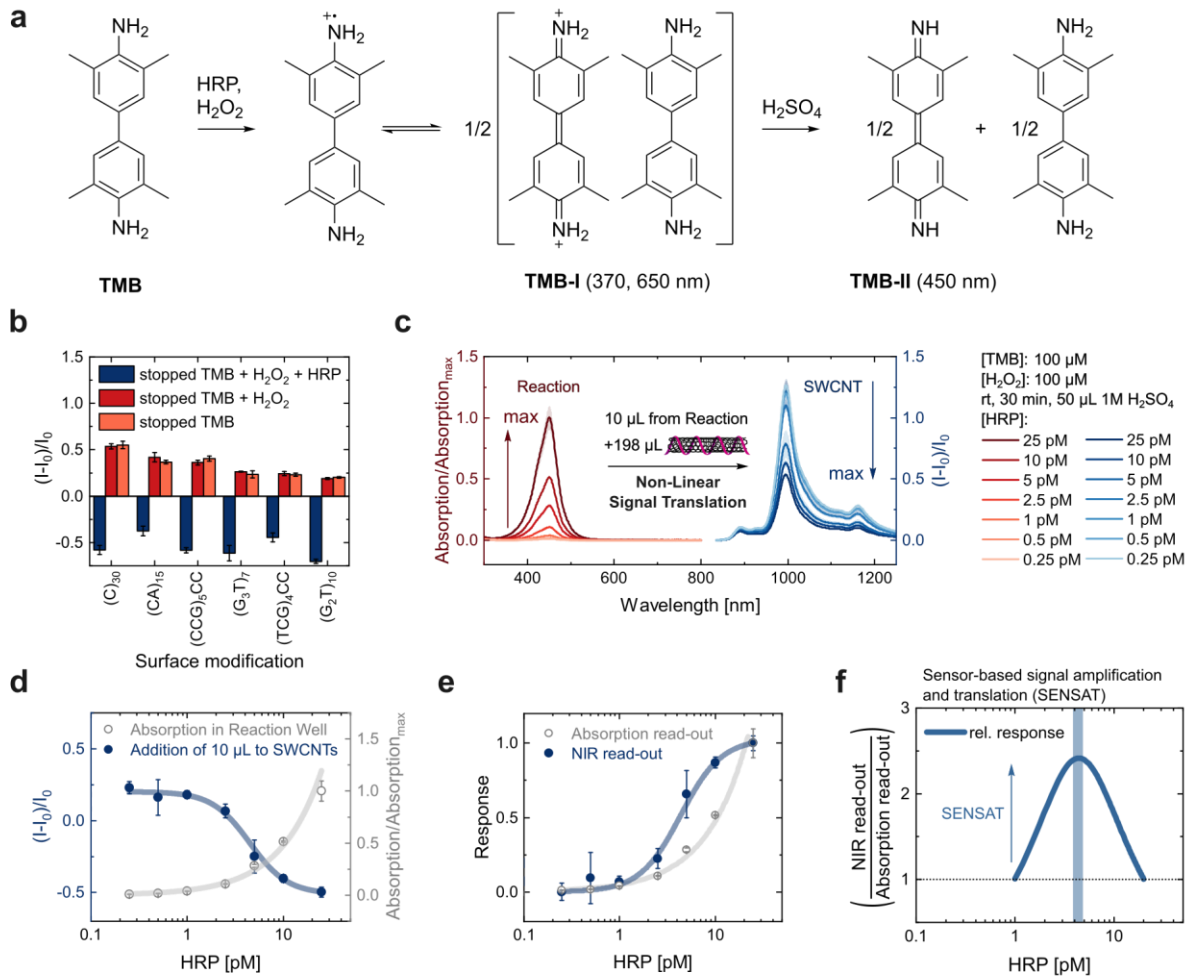

Figure 5: Monitoring and NIR translation of HRP reactions with TMB substrate. (a) Reaction scheme of the TMB oxidation.[19,77,78] (b) Fluorescence modulation of different SWCNTs (198 µL, 0.5 nM) upon the addition of 2 µL from a solution of TMB (100 µM), incubated for 30 min with and without H_2O_2 (100 µM) and HRP (100 pM) and stopped after 30 min, with 50 µL 1 M H_2SO_4 (n=3, mean ± SD). (c) Signal translation between the reaction read-out in the visible and the NIR regime. The reaction of TMB, H_2O_2 and varying HRP concentration was stopped after 30 min, the absorption (red) was measured and 10 µL, from the reaction volume (total 250 µL) was transferred to a well containing C_{30}-SWCNTs (n=3, mean ± SD). (d) Concentration dependent fluorescence and absorption changes (n=3, mean ± SD). € Relative responses and sensor-based signal enhancement (SENSAT). (f) The fits from both read-outs define the optimal SENSAT window (≈–1 - 20 pM). It is centered around the enzyme concentration causing 50 % response (light blue, mean ± SE), which depends on the enzymatic turnover and the affinity of the products for the nanosensors. Note that (e) and (f) are based on data from (d). Fits are linear for absorption data and modified Langmuir adsorption model (see text). Fit parameters: See table S2-S3.

As for the PPD reactions, we observed a non-linear dependency between the responses generated with the classical and the NIR translated read-out. Based on the absorption spectra (Figure 5c), we first excluded the presence of TMB-I. Consequently, we assumed that only TMB and TMB-II modify the SWCNT fluorescence. Assuming substrate saturation, the TMB-II concentration [A] depends on the conversion rate (k) and the enzyme concentration [HRP]:

$$[A] = k[HRP].$$

For HRP concentrations ≤ 25 pM, we observed a near-linear dependence between the HRP concentration and the absorption of the product (Figure 5c). At higher concentrations, we observed substrate depletion. Therefore, we restricted our analysis to HRP concentrations below 25 pM.

For this concentration range, the data from both methods can be readily described with our adsorption model and a linear equation (Figure 5c). To compare the both approaches, it is convenient to plot the response by normalizing the fluorescence to 0 and 1 and normalizing the absorption to 1. When plotting the response of both methods (Figure 5e), one observes a clear signal amplification in the nanosensor read-outs. Dividing the NIR read-out by the absorption read-out yields an enhancement factor of ≈ 2.5. The maximal signal enhancement is centered around the enzyme concentration causing 50 % of the response (4.35 ± 0.49 pM HRP), which illustrates that SENSAT depends on the affinity for the analyte. This amplification is smaller than the one observed for PPD but we underline that the basic concept of SENSAT remains valid and optimization of reaction conditions could further improve it.

A simulation of SENSAT for a larger parameter space exemplifies the potential for optimized nanosensors (Figure 6). It shows that depending on affinities (K_d values) amplification by multiple orders of magnitude is possible for the pure enzyme products (Figure 6a). In enzymatic reaction conditions this is also possible (Figure 6b) even though our current implementation of SWCNTs-based sensors did only show smaller amplification factors.

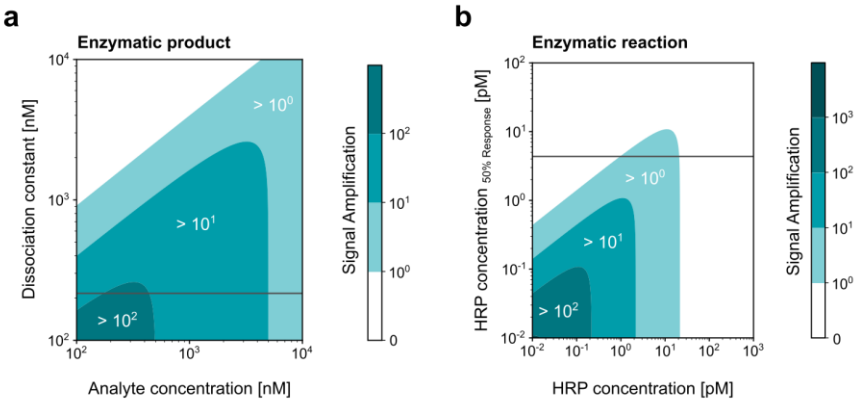

Figure 6: General parameter space for sensor-based signal enhancement and translation (SENSAT) at different experimental conditions. (a) Simulated enhancement by fluorescence relative to absorption. Note that some parameters from figure 3f have been used (BB product, $(G_2T)_{10}$-SWCNT nanosensors (0.1 nM)). (b) Simulated enhancement factor for the whole enzymatic reaction. Note that some parameters from figure 5f have been used (TMB as substrate (100 µM), C_{30}-SWCNT sensors (0.5 nM), stopped after 30 min). The grey reference lines in both plots represent the experimentally determined values. Note that the signal amplification is restricted by the sensor saturation at high concentrations and the lower limit of the sensor.

However, we anticipate that an optimization of reaction conditions including concentrations of the enzyme, buffer conditions, reaction stop conditions etc. will further increase the amplification. Most importantly, the SWCNT surface chemistry could be tailored to find sensors with enhanced affinity for TMB. This could shift amplification into the 10-100x range (Figure 6b). For example, a DNA oligonucleotide with n nucleotides yields 4^n potential variations that will affect sensing.[79,80] Additionally, the introduction of sp^3- and guanine-defects can further extend the chemical space needed for high affinity TMB biosensors.[44,45,81–84] It is therefore likely that unique corona phases with enhanced affinities exist, which further advance the sensing capabilities of nanosensors. Another possibility is to immobilize the nanosensors directly on the ELISA substrate. Recent advances in SWCNT coating showed that long-term stable sterile coatings are possible.[59] Therefore, there are many opportunities to optimize these systems and integrate it into existing standard ELISAs and significantly increase their performance.

Our findings lay the foundation of sensor-based signal amplification and translation (SENSAT) for enzymatic reactions of small molecules. We expect that exploring larger libraries and tailored surface chemistries will further advance the limits of this approach. In this context, highly sensitive nanosensor coatings and the NIR read-out with standard components showcase the potential for rapid integration in ELISAs and western blots.[23,59]

Conclusion

In summary, we present a straightforward method to translate the turnover of enzymatic reactions into the NIR spectrum and amplify the optical signal by using a nanosensor. To this end, we used as model system tailored SWCNTs, which are sensitive to different substrates and products used in typical ELISAs and western blots. Conceptually, this presents a novel approach for a signal translation to a different spectral region with a non-linear signal enhancement that is applicable to any fluorescent sensor/probe. Most importantly, the nanosensor amplifies the signal compared to absorption-based read-outs of colored products. This way it is possible to follow enzymatic reactions in the NIR below the normal limits of detection. The nanosensors can be easily added to and enhance the signal. Therefore, this approach can boost the performance of analytical techniques in which low detection limits of the enzymatic substrates and products are desirable.

Acknowledgements

This work is funded by the Deutsche Forschungsgemeinschaft (DFG, German Research Foundation) under Germany's Excellence Strategy—EXC 2033–390677874—RESOLV. We are also grateful for the support of the VW foundation. This work was further supported by the "Center for Solvation Science ZEMOS" funded by the German Federal Ministry of Education and Research BMBF, and by the Ministry of Culture and Research of Nord Rhine-Westphalia, as well as by the Fraunhofer Internal Programs under Grant No. Attract 038–610097. We thank Dr. Sebastian Jung for access and his technical support with the plate reader.

Conflict of Interest

S.K., J.T.M., and S.H. are listed as inventors on a patent application describing the sensors and the signal translation presented in this study.

References

(1) Cohen, L.; Walt, D. R. Highly Sensitive and Multiplexed Protein Measurements. *Chem. Rev.* **2019**, *119* (1), 293–321. DOI: 10.1021/acs.chemrev.8b00257.

(2) Engvall, E.; Perlmann, P. Enzyme-linked immunosorbent assay (ELISA). Quantitative assay of immunoglobulin G. *Immunochemistry* **1971**, *8* (9), 871–874. DOI: 10.1016/0019-2791(71)90454-x.

(3) Lequin, R. M. Enzyme immunoassay (EIA)/enzyme-linked immunosorbent assay (ELISA). *Clin. Chem.* **2005**, *51* (12), 2415–2418. DOI: 10.1373/clinchem.2005.051532.

(4) Burnette, W. N. "Western blotting": electrophoretic transfer of proteins from sodium dodecyl sulfate--polyacrylamide gels to unmodified nitrocellulose and radiographic detection with antibody and radioiodinated protein A. *Anal. Biochem.* **1981**, *112* (2), 195–203. DOI: 10.1016/0003-2697(81)90281-5.

(5) Kurien, B. T.; Scofield, R. H. Western blotting. *Methods* **2006**, *38* (4), 283–293. DOI: 10.1016/j.ymeth.2005.11.007.

(6) Renart, J.; Reiser, J.; Stark, G. R. Transfer of proteins from gels to diazobenzyloxymethyl-paper and detection with antisera: a method for studying antibody specificity and antigen structure. *PNAS* **1979**, *76* (7), 3116–3120. DOI: 10.1073/pnas.76.7.3116.

(7) Towbin, H.; Staehelin, T.; Gordon, J. Electrophoretic transfer of proteins from polyacrylamide gels to nitrocellulose sheets: procedure and some applications. *PNAS* **1979**, *76* (9), 4350–4354. DOI: 10.1073/pnas.76.9.4350.

(8) Voller, A.; Bartlett, A.; Bidwell, D. E. Enzyme immunoassays with special reference to ELISA techniques. *J. Clin. Pathol.* **1978**, *31* (6), 507–520. DOI: 10.1136/jcp.31.6.507.

(9) Mahmood, T.; Yang, P.-C. Western blot: technique, theory, and trouble shooting. *N. Am. J. Med. Sci.* **2012**, *4* (9), 429–434. DOI: 10.4103/1947-2714.100998.
(10) Rissin, D. M.; Kan, C. W.; Song, L.; Rivnak, A. J.; Fishburn, M. W.; Shao, Q.; Piech, T.; Ferrell, E. P.; Meyer, R. E.; Campbell, T. G.; Fournier, D. R.; Duffy, D. C. Multiplexed single molecule immunoassays. *Lab Chip* **2013**, *13* (15), 2902–2911. DOI: 10.1039/c3lc50416f.
(11) Rissin, D. M.; Kan, C. W.; Campbell, T. G.; Howes, S. C.; Fournier, D. R.; Song, L.; Piech, T.; Patel, P. P.; Chang, L.; Rivnak, A. J.; Ferrell, E. P.; Randall, J. D.; Provuncher, G. K.; Walt, D. R.; Duffy, D. C. Single-molecule enzyme-linked immunosorbent assay detects serum proteins at subfemtomolar concentrations. *Nat. Biotechnol.* **2010**, *28* (6), 595–599. DOI: 10.1038/nbt.1641.
(12) Rissin, D. M.; Fournier, D. R.; Piech, T.; Kan, C. W.; Campbell, T. G.; Song, L.; Chang, L.; Rivnak, A. J.; Patel, P. P.; Provuncher, G. K.; Ferrell, E. P.; Howes, S. C.; Pink, B. A.; Minnehan, K. A.; Wilson, D. H.; Duffy, D. C. Simultaneous detection of single molecules and singulated ensembles of molecules enables immunoassays with broad dynamic range. *Anal. Chem.* **2011**, *83* (6), 2279–2285. DOI: 10.1021/ac103161b.
(13) Mickert, M. J.; Farka, Z.; Kostiv, U.; Hlaváček, A.; Horák, D.; Skládal, P.; Gorris, H. H. Measurement of Sub-femtomolar Concentrations of Prostate-Specific Antigen through Single-Molecule Counting with an Upconversion-Linked Immunosorbent Assay. *Anal. Chem.* **2019**, *91* (15), 9435–9441. DOI: 10.1021/acs.analchem.9b02872.
(14) Brandmeier, J. C.; Jurga, N.; Grzyb, T.; Hlaváček, A.; Obořilová, R.; Skládal, P.; Farka, Z.; Gorris, H. H. Digital and Analog Detection of SARS-CoV-2 Nucleocapsid Protein via an Upconversion-Linked Immunosorbent Assay. *Anal. Chem.* **2023**, *95* (10), 4753–4759. DOI: 10.1021/acs.analchem.2c05670.
(15) Saa, L.; Virel, A.; Sanchez-Lopez, J.; Pavlov, V. Analytical applications of enzymatic growth of quantum dots. *Chemistry* **2010**, *16* (21), 6187–6192. DOI: 10.1002/chem.200903373.
(16) Saa, L.; Pavlov, V. Enzymatic growth of quantum dots: applications to probe glucose oxidase and horseradish peroxidase and sense glucose. *Small* **2012**, *8* (22), 3449–3455. DOI: 10.1002/smll.201201364.
(17) Malashikhina, N.; Garai-Ibabe, G.; Pavlov, V. Unconventional application of conventional enzymatic substrate: first fluorogenic immunoassay based on enzymatic formation of quantum dots. *Anal. Chem.* **2013**, *85* (14), 6866–6870. DOI: 10.1021/ac4011342.
(18) Wang, J.; Liu, G.; Jan, M. R. Ultrasensitive electrical biosensing of proteins and DNA: carbon-nanotube derived amplification of the recognition and transduction events. *J. Am. Chem. Soc.* **2004**, *126* (10), 3010–3011. DOI: 10.1021/ja031723w.
(19) Zhang, X.; Yang, Q.; Lang, Y.; Jiang, X.; Wu, P. Rationale of 3,3',5,5'-Tetramethylbenzidine as the Chromogenic Substrate in Colorimetric Analysis. *Anal. Chem.* **2020**, *92* (18), 12400–12406. DOI: 10.1021/acs.analchem.0c02149.
(20) O'Connell, M. J.; Bachilo, S. M.; Huffman, C. B.; Moore, V. C.; Strano, M. S.; Haroz, E. H.; Rialon, K. L.; Boul, P. J.; Noon, W. H.; Kittrell, C.; Ma, J.; Hauge, R. H.; Weisman, R. B.; Smalley, R. E. Band gap fluorescence from individual single-walled carbon nanotubes. *Science* **2002**, *297* (5581), 593–596. DOI: 10.1126/science.1072631.
(21) Hong, G.; Antaris, A. L.; Dai, H. Near-infrared fluorophores for biomedical imaging. *Nat. Biomed. Eng.* **2017**, *1* (1), 1–22. DOI: 10.1038/s41551-016-0010.
(22) Chen, Y.; Wang, S.; Zhang, F. Near-infrared luminescence high-contrast in vivo biomedical imaging. *Nat. Rev. Bioeng.* **2023**, *1* (1), 60–78. DOI: 10.1038/s44222-022-00002-8.
(23) Ackermann, J.; Stegemann, J.; Smola, T.; Reger, E.; Jung, S.; Schmitz, A.; Herbertz, S.; Erpenbeck, L.; Seidl, K.; Kruss, S. High Sensitivity Near-Infrared Imaging of Fluorescent Nanosensors. *Small* **2023**, *19* (14), e2206856. DOI: 10.1002/smll.202206856.
(24) Ackermann, J.; Metternich, J. T.; Herbertz, S.; Kruss, S. Biosensing with Fluorescent Carbon Nanotubes. *Angew. Chem. Int. Ed.* **2022.** DOI: 10.1002/anie.202112372.
(25) Birkmeier, K.; Hertel, T.; Hartschuh, A. Probing the ultrafast dynamics of excitons in single semiconducting carbon nanotubes. *Nat. Commun.* **2022**, *13* (1), 6290. DOI: 10.1038/s41467-022-33941-2.
(26) Zaumseil, J. Luminescent Defects in Single‐Walled Carbon Nanotubes for Applications. *Adv. Opt. Mater.* **2022**, *10* (2), 2101576. DOI: 10.1002/adom.202101576.
(27) Paviolo, C.; Cognet, L. Near-infrared nanoscopy with carbon-based nanoparticles for the exploration of the brain extracellular space. *Neurobiol. Dis.* **2021**, *153*, 105328. DOI: 10.1016/j.nbd.2021.105328.
(28) Kruss, S.; Hilmer, A. J.; Zhang, J.; Reuel, N. F.; Mu, B.; Strano, M. S. Carbon nanotubes as optical biomedical sensors. *Adv. Drug Deliv. Rev.* **2013**, *65* (15), 1933–1950. DOI: 10.1016/j.addr.2013.07.015.
(29) Gillen, A. J.; Boghossian, A. A. Non-covalent Methods of Engineering Optical Sensors Based on Single-Walled Carbon Nanotubes. *Front. Chem.* **2019**, *7*, 612. DOI: 10.3389/fchem.2019.00612.
(30) Hong, G.; Diao, S.; Antaris, A. L.; Dai, H. Carbon Nanomaterials for Biological Imaging and Nanomedicinal Therapy. *Chem. Rev.* **2015**, *115* (19), 10816–10906. DOI: 10.1021/acs.chemrev.5b00008.
(31) Schroeder, V.; Savagatrup, S.; He, M.; Lin, S.; Swager, T. M. Carbon Nanotube Chemical Sensors. *Chem. Rev.* **2019**, *119* (1), 599–663. DOI: 10.1021/acs.chemrev.8b00340.
(32) Gillen, A. J.; Boghossian, A. A. Non-covalent Methods of Engineering Optical Sensors Based on Single-Walled Carbon Nanotubes. *Front. Chem.* **2019**, *7*, 612. DOI: 10.3389/fchem.2019.00612.
(33) Ernst, F.; Heek, T.; Setaro, A.; Haag, R.; Reich, S. Functional Surfactants for Carbon Nanotubes: Effects of Design. *J. Phys. Chem. C* **2013**, *117* (2), 1157–1162. DOI: 10.1021/jp3098186.
(34) Zheng, M.; Jagota, A.; Semke, E. D.; Diner, B. A.; McLean, R. S.; Lustig, S. R.; Richardson, R. E.; Tassi, N. G. DNA-assisted dispersion and separation of carbon nanotubes. *Nat. Mater.* **2003**, *2* (5), 338–342. DOI: 10.1038/nmat877.
(35) Zheng, M.; Jagota, A.; Strano, M. S.; Santos, A. P.; Barone, P.; Chou, S. G.; Diner, B. A.; Dresselhaus, M. S.; McLean, R. S.; Onoa, G. B.; Samsonidze, G. G.; Semke, E. D.; Usrey, M.; Walls, D. J. Structure-based carbon nanotube sorting by sequence-dependent DNA assembly. *Science* **2003**, *302* (5650), 1545–1548. DOI: 10.1126/science.1091911.

(36) Zhang, J.; Landry, M. P.; Barone, P. W.; Kim, J.-H.; Lin, S.; Ulissi, Z. W.; Lin, D.; Mu, B.; Boghossian, A. A.; Hilmer, A. J.; Rwei, A.; Hinckley, A. C.; Kruss, S.; Shandell, M. A.; Nair, N.; Blake, S.; Şen, F.; Şen, S.; Croy, R. G.; Li, D.; Yum, K.; Ahn, J.-H.; Jin, H.; Heller, D. A.; Essigmann, J. M.; Blankschtein, D.; Strano, M. S. Molecular recognition using corona phase complexes made of synthetic polymers adsorbed on carbon nanotubes. *Nat. Nanotechnol.* **2013**, *8* (12), 959–968. DOI: 10.1038/nnano.2013.236.
(37) Salem, D. P.; Landry, M. P.; Bisker, G.; Ahn, J.; Kruss, S.; Strano, M. S. Chirality dependent corona phase molecular recognition of DNA-wrapped carbon nanotubes. *Carbon* **2016**, *97*, 147–153. DOI: 10.1016/j.carbon.2015.08.075.
(38) Landry, M. P.; Kruss, S.; Nelson, J. T.; Bisker, G.; Iverson, N. M.; Reuel, N. F.; Strano, M. S. Experimental tools to study molecular recognition within the nanoparticle corona. *Sensors* **2014**, *14* (9), 16196–16211. DOI: 10.3390/s140916196.
(39) Bisker, G.; Dong, J.; Park, H. D.; Iverson, N. M.; Ahn, J.; Nelson, J. T.; Landry, M. P.; Kruss, S.; Strano, M. S. Protein-targeted corona phase molecular recognition. *Nat. Commun.* **2016**, *7*, 10241. DOI: 10.1038/ncomms10241.
(40) Wang, H.; Boghossian, A. A. Covalent conjugation of proteins onto fluorescent single-walled carbon nanotubes for biological and medical applications. *Mater. Adv.* **2023**, *4* (3), 823–834. DOI: 10.1039/D2MA00714B.
(41) Jin, X.; Lee, M. A.; Gong, X.; Koman, V. B.; Lundberg, D. J.; Wang, S.; Bakh, N. A.; Park, M.; Dong, J. I.; Kozawa, D.; Cho, S.-Y.; Strano, M. S. Corona Phase Molecular Recognition of the Interleukin-6 (IL-6) Family of Cytokines Using nIR Fluorescent Single-Walled Carbon Nanotubes. *ACS Appl. Nano Mater.* **2023**, *6* (11), 9791–9804. DOI: 10.1021/acsanm.3c01525.
(42) Williams, R. M.; Lee, C.; Galassi, T. V.; Harvey, J. D.; Leicher, R.; Sirenko, M.; Dorso, M. A.; Shah, J.; Olvera, N.; Dao, F.; Levine, D. A.; Heller, D. A. Noninvasive ovarian cancer biomarker detection via an optical nanosensor implant. *Sci. Adv.* **2018**, *4* (4), eaaq1090. DOI: 10.1126/sciadv.aaq1090.
(43) Gaikwad, P.; Rahman, N.; Parikh, R.; Crespo, J.; Cohen, Z.; Williams, R. Optical nanosensor passivation enables highly sensitive detection of the inflammatory cytokine IL-6. *bioRxiv* **2023.** DOI: 10.1101/2023.05.10.540217. Published Online: 05-2023.
(44) Kim, M.; Chen, C.; Wang, P.; Mulvey, J. J.; Yang, Y.; Wun, C.; Antman-Passig, M.; Luo, H.-B.; Cho, S.; Long-Roche, K.; Ramanathan, L. V.; Jagota, A.; Zheng, M.; Wang, Y.; Heller, D. A. Detection of ovarian cancer via the spectral fingerprinting of quantum-defect-modified carbon nanotubes in serum by machine learning. *Nat. Biomed. Eng.* **2022**, *6* (3), 267–275. DOI: 10.1038/s41551-022-00860-y.
(45) Metternich, J. T.; Wartmann, J. A. C.; Sistemich, L.; Nißler, R.; Herbertz, S.; Kruss, S. Near-Infrared Fluorescent Biosensors Based on Covalent DNA Anchors. *J. Am. Chem. Soc.* **2023**, *145* (27), 14776–14783. DOI: 10.1021/jacs.3c03336.
(46) Kuo, M.-T.; Raffaelle, J. F.; Waller, E. M.; Varaljay, V. A.; Wagner, D.; Kelley-Loughnane, N.; Reuel, N. F. Screening Enzymatic Degradation of Polyester Polyurethane with Fluorescent Single-walled Carbon Nanotube and Polymer Nanoparticle Conjugates. *ACS Nano* **2023.** DOI: 10.1021/acsnano.3c04347.
(47) Freeley, M.; Worthy, H. L.; Ahmed, R.; Bowen, B.; Watkins, D.; Macdonald, J. E.; Zheng, M.; Jones, D. D.; Palma, M. Site-Specific One-to-One Click Coupling of Single Proteins to Individual Carbon Nanotubes: A Single-Molecule Approach. *J. Am. Chem. Soc.* **2017**, *139* (49), 17834–17840. DOI: 10.1021/jacs.7b07362.
(48) Kallmyer, N. E.; Musielewicz, J.; Sutter, J.; Reuel, N. F. Substrate-Wrapped, Single-Walled Carbon Nanotube Probes for Hydrolytic Enzyme Characterization. *Anal. Chem.* **2018**, *90* (8), 5209–5216. DOI: 10.1021/acs.analchem.7b05444.
(49) Harvey, J. D.; Jena, P. V.; Baker, H. A.; Zerze, G. H.; Williams, R. M.; Galassi, T. V.; Roxbury, D.; Mittal, J.; Heller, D. A. A Carbon Nanotube Reporter of miRNA Hybridization Events In Vivo. *Nat. Biomed. Eng.* **2017**, *1*, 1–11. DOI: 10.1038/s41551-017-0041.
(50) Harvey, J. D.; Baker, H. A.; Ortiz, M. V.; Kentsis, A.; Heller, D. A. HIV Detection via a Carbon Nanotube RNA Sensor. *ACS Sens.* **2019**, *4* (5), 1236–1244. DOI: 10.1021/acssensors.9b00025.
(51) Amoroso, G.; Ye, Q.; Cervantes-Salguero, K.; Fernández, G.; Cecconello, A.; Palma, M. DNA-Powered Stimuli-Responsive Single-Walled Carbon Nanotube Junctions. *Chem. Mater.* **2019**, *31* (5), 1537–1542. DOI: 10.1021/acs.chemmater.8b04483.
(52) Hendler-Neumark, A.; Wulf, V.; Bisker, G. Single-Walled Carbon Nanotube Sensor Selection for the Detection of MicroRNA Biomarkers for Acute Myocardial Infarction as a Case Study. *ACS Sens.* **2023.** DOI: 10.1021/acssensors.3c00633.
(53) Jeng, E. S.; Nelson, J. D.; Prather, K. L. J.; Strano, M. S. Detection of a single nucleotide polymorphism using single-walled carbon-nanotube near-infrared fluorescence. *Small* **2010**, *6* (1), 40–43. DOI: 10.1002/smll.200900944.
(54) Cui, J.; Gong, X.; Cho, S.-Y.; Jin, X.; Yang, S.; Khosravi-Far, R.; Strano, M. S. Understanding Oligonucleotide Hybridization and the Role of Anchoring on the Single-Walled Carbon Nanotube Corona Phase for Viral Sensing Applications. *J. Phys. Chem. C* **2022.** DOI: 10.1021/acs.jpcc.2c06434.
(55) Polo, E.; Kruss, S. Nanosensors for neurotransmitters. *Anal. Bioanal. Chem.* **2016**, *408* (11), 2727–2741. DOI: 10.1007/s00216-015-9160-x.
(56) Kruss, S.; Landry, M. P.; Vander Ende, E.; Lima, B. M. A.; Reuel, N. F.; Zhang, J.; Nelson, J.; Mu, B.; Hilmer, A.; Strano, M. Neurotransmitter detection using corona phase molecular recognition on fluorescent single-walled carbon nanotube sensors. *J. Am. Chem. Soc.* **2014**, *136* (2), 713–724. DOI: 10.1021/ja410433b.
(57) Elizarova, S.; Chouaib, A. A.; Shaib, A.; Hill, B.; Mann, F.; Brose, N.; Kruss, S.; Daniel, J. A. A fluorescent nanosensor paint detects dopamine release at axonal varicosities with high spatiotemporal resolution. *PNAS* **2022**, *119* (22), e2202842119. DOI: 10.1073/pnas.2202842119.
(58) Dinarvand, M.; Elizarova, S.; Daniel, J.; Kruss, S. Imaging of Monoamine Neurotransmitters with Fluorescent Nanoscale Sensors. *ChemPlusChem* **2020**, *85* (7), 1465–1480. DOI: 10.1002/cplu.202000248.
(59) Ackermann, J.; Reger, E.; Jung, S.; Mohr, J.; Herbertz, S.; Seidl, K.; Kruss, S. Smart Slides for Optical Monitoring of Cellular Processes. *Adv. Funct. Mater.* **2023.** DOI: 10.1002/adfm.202309064.

(60) Wu, H.; Nißler, R.; Morris, V.; Herrmann, N.; Hu, P.; Jeon, S.-J.; Kruss, S.; Giraldo, J. P. Monitoring Plant Health with Near-Infrared Fluorescent H2O2 Nanosensors. *Nano Lett.* **2020**, *20* (4), 2432–2442. DOI: 10.1021/acs.nanolett.9b05159.
(61) Kim, J.-H.; Heller, D. A.; Jin, H.; Barone, P. W.; Song, C.; Zhang, J.; Trudel, L. J.; Wogan, G. N.; Tannenbaum, S. R.; Strano, M. S. The rational design of nitric oxide selectivity in single-walled carbon nanotube near-infrared fluorescence sensors for biological detection. *Nat. Chem.* **2009**, *1* (6), 473–481. DOI: 10.1038/nchem.332.
(62) Meier, J.; Stapleton, J.; Hofferber, E.; Haworth, A.; Kachman, S.; Iverson, N. M. Quantification of Nitric Oxide Concentration Using Single-Walled Carbon Nanotube Sensors. *Nanomater.* **2021**, *11* (1), 243. DOI: 10.3390/nano11010243.
(63) Ulissi, Z. W.; Sen, F.; Gong, X.; Sen, S.; Iverson, N.; Boghossian, A. A.; Godoy, L. C.; Wogan, G. N.; Mukhopadhyay, D.; Strano, M. S. Spatiotemporal intracellular nitric oxide signaling captured using internalized, near-infrared fluorescent carbon nanotube nanosensors. *Nano Lett.* **2014**, *14* (8), 4887–4894. DOI: 10.1021/nl502338y.
(64) Giraldo, J. P.; Landry, M. P.; Kwak, S.-Y.; Jain, R. M.; Wong, M. H.; Iverson, N. M.; Ben-Naim, M.; Strano, M. S. A Ratiometric Sensor Using Single Chirality Near-Infrared Fluorescent Carbon Nanotubes: Application to In Vivo Monitoring. *Small* **2015**, *11* (32), 3973–3984. DOI: 10.1002/smll.201403276.
(65) Safaee, M. M.; Gravely, M.; Roxbury, D. A Wearable Optical Microfibrous Biomaterial with Encapsulated Nanosensors Enables Wireless Monitoring of Oxidative Stress. *Adv. Funct. Mater.* **2021**, *31* (13), 2006254. DOI: 10.1002/adfm.202006254.
(66) Ang, M. C.-Y.; Dhar, N.; Khong, D. T.; Lew, T. T. S.; Park, M.; Sarangapani, S.; Cui, J.; Dehadrai, A.; Singh, G. P.; Chan-Park, M. B.; Sarojam, R.; Strano, M. Nanosensor Detection of Synthetic Auxins In Planta using Corona Phase Molecular Recognition. *ACS Sens.* **2021**, *6* (8), 3032–3046. DOI: 10.1021/acssensors.1c01022.
(67) Dong, J.; Lee, M. A.; Rajan, A. G.; Rahaman, I.; Sun, J. H.; Park, M.; Salem, D. P.; Strano, M. S. A synthetic mimic of phosphodiesterase type 5 based on corona phase molecular recognition of single-walled carbon nanotubes. *PNAS* **2020**, *117* (43), 26616–26625. DOI: 10.1073/pnas.1920352117.
(68) Nißler, R.; Müller, A. T.; Dohrman, F.; Kurth, L.; Li, H.; Cosio, E. G.; Flavel, B. S.; Giraldo, J. P.; Mithöfer, A.; Kruss, S. Detection and imaging of the plant pathogen response by near infrared fluorescent polyphenol sensors. *Angew. Chem. Int. Ed.* **2021.** DOI: 10.1002/anie.202108373.
(69) Amir, D.; Hendler‐Neumark, A.; Wulf, V.; Ehrlich, R.; Bisker, G. Oncometabolite Fingerprinting Using Fluorescent Single‐Walled Carbon Nanotubes. *Adv Materials Inter* **2022**, *9* (4). DOI: 10.1002/admi.202101591.
(70) Wong, M. H.; Giraldo, J. P.; Kwak, S.-Y.; Koman, V. B.; Sinclair, R.; Lew, T. T. S.; Bisker, G.; Liu, P.; Strano, M. S. Nitroaromatic detection and infrared communication from wild-type plants using plant nanobionics. *Nat. Mater.* **2017**, *16* (2), 264–272. DOI: 10.1038/NMAT4771.
(71) Shiraki, T.; Onitsuka, H.; Shiraishi, T.; Nakashima, N. Near infrared photoluminescence modulation of single-walled carbon nanotubes based on a molecular recognition approach. *Chem. Commun.* **2016**, *52* (88), 12972–12975. DOI: 10.1039/C6CC07287A.
(72) Cognet, L.; Tsyboulski, D. A.; Rocha, J.-D. R.; Doyle, C. D.; Tour, J. M.; Weisman, R. B. Stepwise quenching of exciton fluorescence in carbon nanotubes by single-molecule reactions. *Science* **2007**, *316* (5830), 1465–1468. DOI: 10.1126/science.1141316.
(73) Zhang, J.; Boghossian, A. A.; Barone, P. W.; Rwei, A.; Kim, J.-H.; Lin, D.; Heller, D. A.; Hilmer, A. J.; Nair, N.; Reuel, N. F.; Strano, M. S. Single molecule detection of nitric oxide enabled by d(AT)15 DNA adsorbed to near infrared fluorescent single-walled carbon nanotubes. *J. Am. Chem. Soc.* **2011**, *133* (3), 567–581. DOI: 10.1021/ja1084942.
(74) Kruss, S.; Salem, D. P.; Vuković, L.; Lima, B.; Vander Ende, E.; Boyden, E. S.; Strano, M. S. High-resolution imaging of cellular dopamine efflux using a fluorescent nanosensor array. *PNAS* **2017**, *114* (8), 1789–1794. DOI: 10.1073/pnas.1613541114.
(75) Gong, X.; Kwak, S.-Y.; Cho, S.-Y.; Lundberg, D.; Liu, A. T.; McGee, M. K.; Strano, M. S. Single-Molecule Methane Sensing Using Palladium-Functionalized nIR Fluorescent Single-Walled Carbon Nanotubes. *ACS Sens.* **2023.** DOI: 10.1021/acssensors.3c01542.
(76) Berger, F. J.; Sousa, J. A. de; Zhao, S.; Zorn, N. F.; El Yumin, A. A.; Quintana García, A.; Settele, S.; Högele, A.; Crivillers, N.; Zaumseil, J. Interaction of Luminescent Defects in Carbon Nanotubes with Covalently Attached Stable Organic Radicals. *ACS Nano* **2021**, *15* (3), 5147–5157. DOI: 10.1021/acsnano.0c10341.
(77) Josephy, P. D.; Eling, T.; Mason, R. P. The horseradish peroxidase-catalyzed oxidation of 3,5,3',5'-tetramethylbenzidine. Free radical and charge-transfer complex intermediates. *J. Biol. Chem.* **1982**, *257* (7), 3669–3675. DOI: 10.1016/S0021-9258(18)34832-4.
(78) Frey, A.; Meckelein, B.; Externest, D.; Schmidt, M. A. A stable and highly sensitive 3,3',5,5'-tetramethylbenzidine-based substrate reagent for enzyme-linked immunosorbent assays. *J. Immunol. Methods* **2000**, *233* (1-2), 47–56. DOI: 10.1016/S0022-1759(99)00166-0.
(79) Tu, X.; Manohar, S.; Jagota, A.; Zheng, M. DNA sequence motifs for structure-specific recognition and separation of carbon nanotubes. *Nature* **2009**, *460* (7252), 250–253. DOI: 10.1038/nature08116.
(80) Roxbury, D.; Tu, X.; Zheng, M.; Jagota, A. Recognition ability of DNA for carbon nanotubes correlates with their binding affinity. *Langmuir* **2011**, *27* (13), 8282–8293. DOI: 10.1021/la2007793.
(81) Mann, F. A.; Herrmann, N.; Opazo, F.; Kruss, S. Quantum Defects as a Toolbox for the Covalent Functionalization of Carbon Nanotubes with Peptides and Proteins. *Angew. Chem. Int. Ed.* **2020**, *59* (40), 17732–17738. DOI: 10.1002/anie.202003825.
(82) Zheng, Y.; Bachilo, S. M.; Weisman, R. B. Controlled Patterning of Carbon Nanotube Energy Levels by Covalent DNA Functionalization. *ACS Nano* **2019**, *13* (7), 8222–8228. DOI: 10.1021/acsnano.9b03488.
(83) Galonska, P.; Mohr, J. M.; Schrage, C. A.; Schnitzler, L.; Kruss, S. Guanine Quantum Defects in Carbon Nanotubes for Biosensing. *J. Phys. Chem. Lett.* **2023**, *14* (14), 3483–3490. DOI: 10.1021/acs.jpclett.3c00358.

(84) Lin, Z.; Beltran, L. C.; Los Santos, Z. A. de; Li, Y.; Adel, T.; Fagan, J. A.; Hight Walker, A. R.; Egelman, E. H.; Zheng, M. DNA-guided lattice remodeling of carbon nanotubes. *Science* **2022**, *377* (6605), 535–539. DOI: 10.1126/science.abo4628.

Graphical Abstract

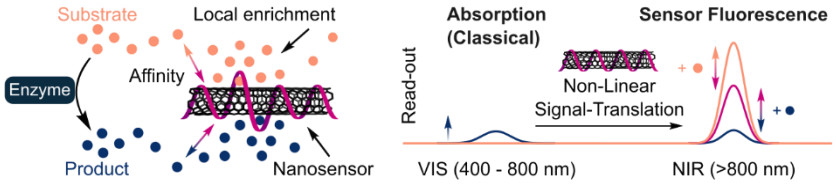

ELISA substrates and products modulate the near-infrared fluorescence of single-walled carbon nanotubes (SWCNTs) modified with specific (bio)polymers. The affinity of these nanosensors for the analyte increases the effective local concentration compared to normal absorption measurements. This causes a signal enhancement, which improves the readout of enzymatic reactions.